Molecular Crystals and Liquid Crystals
Publication details, including instructions for authors and subscription information:
http://www.tandfonline.com/loi/gmcl20

Field Induced Helix Anharmonicity and Fast In-Plane Electrooptic Switching of Chiral Liquid Crystals

S. P. Palto [a], M. I. Barnik [a], L. M. Blinov [a], B. A. Umanskii [a] & N. M. Shtykov [a]

[a] Institute of Crystallography, Russian Academy of Sciences, Moscow, Russia

Version of record first published: 14 Jun 2011

To cite this article: S. P. Palto, M. I. Barnik, L. M. Blinov, B. A. Umanskii & N. M. Shtykov (2011): Field Induced Helix Anharmonicity and Fast In-Plane Electrooptic Switching of Chiral Liquid Crystals, Molecular Crystals and Liquid Crystals, 544:1, 119/[1107]-135/[1123]

To link to this article: http://dx.doi.org/10.1080/15421406.2011.569284

Mol. Cryst. Liq. Cryst., Vol. 544: pp. 119/[1107]–135/[1123], 2011

ISSN: 1542-1406 print/1563-5287 online
DOI: 10.1080/15421406.2011.569284

Taylor & Francis
Taylor & Francis Group

Field Induced Helix Anharmonicity and Fast In-Plane Electrooptic Switching of Chiral Liquid Crystals

S. P. PALTO, M. I. BARNIK, L. M. BLINOV, B. A. UMANSKII, AND N. M. SHTYKOV

Institute of Crystallography, Russian Academy of Sciences, Moscow, Russia

Polarization, spectral and relaxation properties of a new electrooptic effect in aligned layers of chiral nematic liquid crystals are considered. The physical mechanism of the effect is based on the emergence of high spatial harmonics in the helical structure of the director field, which determine a high rate of the electrooptic response. An effective control of spectral properties of the corresponding devices is performed using variations of the optical anisotropy and the helical pitch of a liquid crystal.

Keywords Chiral liquid crystals; fast electro-optic effects; in-plane-switching; induced helix anharmonicity

1. Introduction

Among a variety of liquid crystals (LC) of special interest are chiral phases with a spontaneous helical distribution of the director (local optical axis) of the LC. The helical distribution of the director, combined with the optical anisotropy of a LC results in a series of optical effects attractive from both fundamental and practical viewpoints. For example, in the range of light wavelengths comparable with the helical pitch $\lambda \approx P_0$, the optical properties characteristic of one-dimensional photonic crystals (particularly, a spectral bandgap) are observed [1,2]. The other regime, $\lambda \ll P_0$, is widely used in electrooptic applications of chiral liquid crystals. In that case, a linear polarization of the eigenmodes propagating along the helical axis synchronously rotates together with the director (Mauguin regime [3]). In the present paper we consider an intermediate case. On the one hand, the helical pitch is considerably larger than wavelengths of the visible light; on the other hand it is short enough for light polarization not to follow the Mauguin regime. The intermediate situation results in the fast electrooptic response and specific spectral properties discussed below in detail.

Address correspondence to S. P. Palto, Institute of Crystallography, Russian Academy of Sciences, Leninsky Prospect 59, Moscow 119333, Russia. Tel.: +7l(495)330-78-47; Fax: +7(495)330-78-47; E-mail: palto@online.ru

Due to anisotropy of physical properties, the electrooptical effects in liquid crystals strongly depend on the direction of the applied electric field vector. One can distinguish between two basic geometries. In the first one, a liquid crystal layer is confined between two transparent electrodes and the applied voltage creates a field along the normal to the layer. In the second geometry, the electric field lies in the layer plane that calls for more complicated and expensive systems of electrodes on the substrates. Nowadays, despite the complexity, the second, so-called In-Plane Switching (IPS) regime becomes very popular due to specific properties of corresponding electrooptic devices.

The electrooptic studies of thin nematic layers in the IPS regime have a 30 years history. One of the earliest works dealt with dynamic light scattering [4]. Later Soref [5] studied IPS-regime with different boundary conditions (planar, homeotropic, etc.). Then similar investigations were carried out on ferroelectric liquid crystals [6,7]. To date the electrooptic effects based on the orientational phenomena in nematics are well understood and find applications to technology for improving angular characteristics of displays [8,9]. As to the chiral nematics, the IPS regime was studied [10] in a planar Grandjean texture with a helical axis perpendicular to the liquid crystal layer and the in-plane electric field applied from a pair of 10 μm thick electrodes. The field induced birefringence observed was discussed in terms of the two effects, namely, the helix unwinding and flexoelectric distortion.

In the present work, we discuss a new electrooptic IPS mode observed in the planar texture of chiral nematics having a helical pitch exceeding visible light wavelengths. This mode has no relation to helix unwinding or flexoelectric effect. As will be shown below, due to local dielectric anisotropy, the field action results in appearance of odd spatial harmonics in the initially sinusoidal director distribution. In turn, despite the smallness of the anharmonicity, the latter results in an essential change (up to the orthogonal state) of the polarization of the light beam transmitted through the chiral nematic layer. As high spatial harmonics of the distorted helical structure are characterized by fast relaxation times, the new effect opens the way to fast electrooptic switching with the times, at least, one order of magnitude shorter with respect to other electrooptic modes known for nematics.

2. Numerical Modeling

2.1. *Basic Equations*

The equations describing the dynamics of the director and the corresponding optical response allow analytic solutions only in particular cases, which cannot embrace a variety of conditions one meets in experiment. Therefore, we solve the basic equations numerically using the software developed by one of the authors [11,12]. The description of the macroscopic dynamics of a nematic liquid crystal is based on the concept of the director $\mathbf{n} = (n_x, n_y, n_z)$, that is unit pseudo-vector ($\mathbf{n} \equiv -\mathbf{n}$) following the preferred molecular orientation. In the case of a one-dimensional, non-uniform (in the z-direction) liquid crystal layer, the dynamic of the director field $\mathbf{n}(z)$, with the backflow neglected, is given by numerical solution of equation

$$\gamma \frac{d\mathbf{n}}{dt} = -\frac{\partial F}{\partial \mathbf{n}} + \frac{d}{dz}\left(\frac{\partial F}{\partial \mathbf{n}'}\right) + \lambda \mathbf{n} \tag{1}$$

where γ is rotation viscosity, λ is Lagrange multiplier (due to constraint $\mathbf{n}^2 = 1$), and F is the free energy density including the elastic and electric components:

$$F = \frac{1}{2}\left[K_{11}(div\mathbf{n})^2 + K_{22}(\mathbf{n} \bullet \mathrm{curl}\mathbf{n} + q_0)^2 + K_{33}(\mathbf{n} \times \mathrm{curl}\mathbf{n})^2\right] - \frac{\widehat{\varepsilon}\,\mathbf{E} \bullet \mathbf{E}}{2} \qquad (2)$$

Here, K_{11}, K_{22}, K_{33} are moduli of elasticity for bend, twist and splay distortions, respectively [3]; $\widehat{\varepsilon}$ is tensor of dielectric permittivity, $\mathbf{E}$ is vector of external electric field. The finite value of q_0 is responsible for the unlimited helical structure with natural pitch $P_0 = 2\pi/q_0$ and is of principal importance for chiral nematics. In the confined geometry, Eq. (1) is to be solved on account of boundary conditions given by easy axes directions and anchoring energies at the opposite substrates [12].

The calculations of optical properties are carried out using an algorithm described in detail earlier [11]. For layered media or one-dimensional non-uniform media the precise representation of the Maxwell equations is given by the matrix form [13]

$$\frac{\partial}{\partial z}\Psi = \frac{i\omega}{c}\Delta \cdot \Psi, \qquad (3)$$

where the components of matrix Δ are expressed in terms of the $\widehat{\varepsilon}$-tensor components and the column of the electromagnetic field Ψ is determined by electric ($E_{x,y}$) and magnetic ($H_{x,y}$) components:

$$\Psi = (\, E_x \quad H_y \quad E_y \quad -H_x \,)^T \qquad (4)$$

For an optically anisotropic layer of thickness h, the solution of Eq. (3) is evident:

$$\Psi(h) = \exp(i\omega h\Delta/c)\Psi(0) \equiv P(h)\Psi(0) \qquad (5)$$

Here $\Psi(0)$ and $\Psi(h)$ are columns of the electromagnetic field of frequency ω at the input ($z = 0$) and output ($z = h$) of the layer. Therefore, the problem is reduced to the calculation of the exponential function of matrix Δ and finding matrix $P(h)$. In the case of non-uniform layer of helical liquid crystal one needs a discretization procedure and computing a product of matrices $P_i(h_i)$ for individual sublayers. To this effect, the spatial frequency of discretization should be much larger than q_0. Therefore, within the limits of z-variation by a discrete value h_i the director field may be considered uniform.

The analysis of the light polarization states has been carried out by calculations of the Stokes vector components and their representation on the Poincare sphere. For the light electric vector components

$$\begin{aligned} E_x &= A_x \cos(\omega t - kz + \delta_x) \\ E_y &= A_y \cos(\omega t - kz + \delta_y) \end{aligned} \qquad (6)$$

the Stokes vector components are defined as follows

$$S = \begin{pmatrix} S_0 \\ S_1 \\ S_2 \\ S_3 \end{pmatrix} = \begin{pmatrix} A_x^2 + A_y^2 \\ A_x^2 - A_y^2 \\ 2A_xA_y\cos\delta \\ 2A_xA_y\sin\delta \end{pmatrix} \tag{7}$$

where $\delta = \delta_y - \delta_x$.

In the case of polarised light

$$S_0^2 = S_1^2 + S_2^2 + S_3^2 \tag{8}$$

and any polarization state is represented by a point on the Poincare sphere with radius S_0 equal to intensity of polarized light. Any point at the equator corresponds to linearly polarized light. Points outside the equator map the states of elliptic polarization transformed in the circular ones at the poles of the sphere.

In a thin layer of a chiral liquid crystal with planar boundary conditions, the director continuously rotates about the normal to the layer plane (z-direction) and forms a helix with a pitch P that may differ from the natural pitch P_0 [14,15]. In the electric field absence, the spatial distribution of the director field is described by harmonic functions of the type

$$\mathbf{n}(z) = (n_x(z), n_y(z), 0) = (\sin(2\pi z/P + \varphi_0), \cos(2\pi z/P + \varphi_0), 0); \quad n_x^2 + n_y^2 = 1 \tag{9}$$

where φ_0 is the azimuthal angle of the director at the boundary at $z = 0$. To such a layer, one may apply an electric field perpendicular to the axis of the helix with the field strength lower than the threshold for helix unwinding. Then the helix is conserved but the director field $\mathbf{n}(Z)$ becomes distorted. The distribution of x- and y-components of the director along the z-axis will no longer follow the sinusoidal form because the additional harmonics appear:

$$\begin{aligned} n_x(z) &= A_{1,x}\sin(2\pi z/P + \varphi_0) + \sum_m \left(A_{m,x}\sin 2\pi mz/P + B_{m,x}\cos 2\pi mz/P\right), \\ n_y(z) &= A_{1,y}\cos(2\pi z/P + \varphi_0) + \sum_m \left(A_{m,y}\sin 2\pi mz/P + B_{m,y}\cos 2\pi mz/P\right) \end{aligned} \tag{10}$$

Due to the sine-form initial distribution of the director and its quadratic-type interaction with field E, the latter induces only odd harmonics of a helical structure ($m = 2k + 1$, where k is an integer). The amplitudes of harmonics normalized to the first harmonic amplitude characterize a degree of the induced anharmonicity of the structure.

2.2. *Results of Numerical Modelling*

Figure 1 (above) shows Fourier images of the spatial distribution of the director x-component for the zero field ($E = 0$) and $E = 2\,\mathrm{V/\mu m}$. In the same figure (below), we can see the evolution of the light polarization state at the output of 8 μm thick chiral nematic layer having pitch $P = 1.2\,\mu\mathrm{m}$. The field changes from 0 to $2\,\mathrm{V/\mu m}$ with a

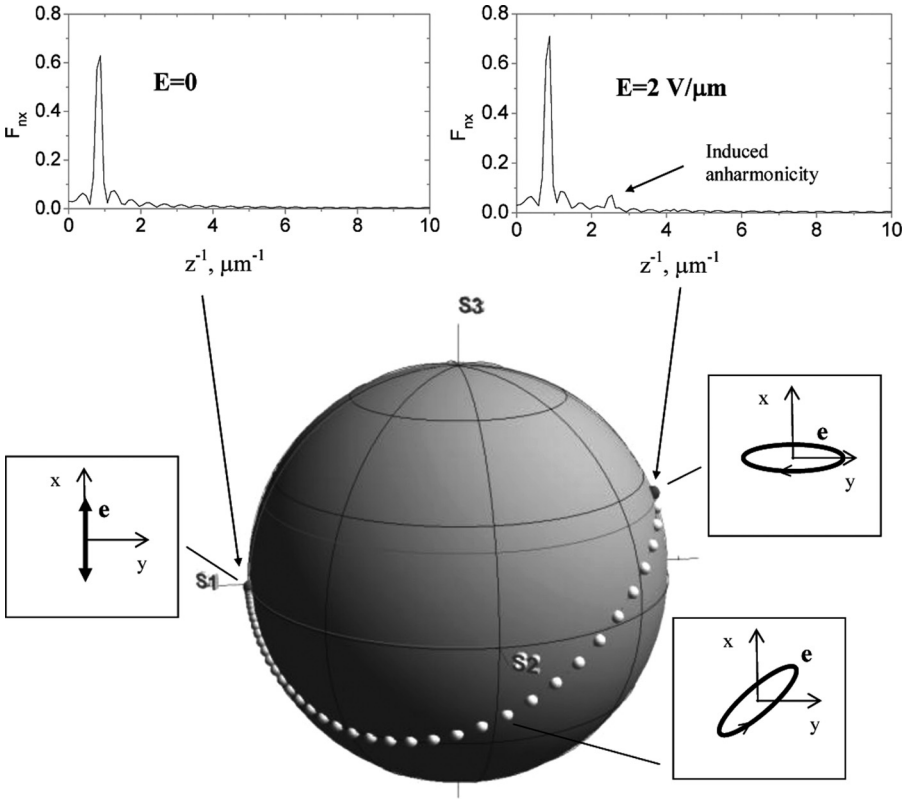

Figure 1. Results of numerical modelling of the effect of induced anharmonicity. Above: Fourier representation of the spatial distribution of the director x-component in the zero field ($E=0$) and in the external field ($E=2\,\mathrm{V}/\mu\mathrm{m}$). Below: the Poincare sphere showing polarization states for the light transmitted through chiral nematic layer parallel to the helical axis upon variation of the field from 0 to $2\,\mathrm{V}/\mu\mathrm{m}$ with step $0.05\,\mathrm{V}/\mu\mathrm{m}$. Azimuthal angles of the director at the borders of the layer at $E=0$ are $\varphi=0$ and -2400 deg. Calculation are made for linearly polarized light with electric vector angle $\alpha=-60$ deg and $\lambda=550\,\mathrm{nm}$.

step of $0.05\,\mathrm{V}/\mu\mathrm{m}$. The parameters for calculation are as follows: twist elastic modulus of $K_{22}=5\mathrm{pN}$, dielectric anisotropy $\Delta\varepsilon=15$, optical anisotropy $\Delta n=n_{\|}-n_{\perp}=0.2$ at wavelength $\lambda=550\,\mathrm{nm}$ ($n_{\|}$ and $n_{\perp}$ are refractive indices for the light propagating along the helical axis with linear polarization parallel or perpendicular to the director). These parameters are typical for real liquid crystals although they may not exactly correspond to our experimental samples, see Table 1. In fact the aim of the modelling was to trace general features of the electrooptic effect and guide the experiment.

In the electric field, the induced anharmonicity mainly manifests itself as the third harmonic of the helix. The ratio of the amplitudes of the 3rd and 1st harmonics (degree of anharmonicity) in the particular example seems to be not high, about 7% at $E=2\,\mathrm{V}/\mu\mathrm{m}$. However, as seen from the points on the Poincare sphere, the light polarization state at the output of liquid crystal layer becomes almost orthogonal to that at the input. In the field absence, the light at the output is linearly polarised and the Stokes vector $(S_0,\ S_1,\ S_2,\ S_3)=(1,1,0,0)$ corresponds to the electric light

Table 1. Codes of experimental samples and their parameters at room temperature (23°C)

Chiral nematics (mixture of nematic and chiral dopant)	Nematics	Concentration of chiral dopant (wt %)	Δn for chiral nematics, $\lambda = 589$ nm	$\Delta\varepsilon$ (1 κГц, for nematics	d (μm) Layer thickness	P, μm
Ch-IPS-2	MLC-6625	6.5	0.075	5.9*	17.5	1 ± 0.1
Ch-IPS-13	E-7	8.4	0.22*	14.5*	17.4	1 ± 0.1
Ch-IPS-15	MLC-6815	15.0	0.0555	2.5	17.5	0.55 ± 0.05
Ch-IPS-16	MLC-6815	8.0	0.0521	2.5	17.4	1 ± 0.1
Ch-IPS-17	MLC-6815	4.0	0.0535	2.5	17.5	2 ± 0.2
Ch-IPS-19	E-7	12.55	0.22*	14.5*	17.5	0.7 ± 0.06
Ch-IPS-20	NP-1565	7.5	0.116	7*	17.5	1 ± 0.1

*Data from the literature or manufacturer at $T = 20$°C.

vector **e** oscillating parallel to x-axis. Therefore, such beam may completely be blocked by an analyser with absorption axis oriented along x. With increasing electric field, the y-component of light vector **e** smoothly grows and the polarization state (point) moves to the opposite side of the Poincare sphere. At $E = 2\,\mathrm{V}/\mu\mathrm{m}$ the point coordinates are $(S_0, S_1, S_2, S_3) = (1, -0.9, 0.16, 0.4)$ and the field-on state is almost orthogonal to the field-off state. Correspondingly, the light intensity after analyser increases and reaches a maximum. In the electric field, the polarization state is not located on the equator of the sphere and the light is elliptically polarised. In fact, the field variation changes both the ratio of the principal axes of the ellipse and their orientation in space.

As said, the polarization of the output light in the zero field may be linear and efficiently blocked by an analyser. From the practical point of view it is very important because, in the field-on regime, high values of the contrast can be achieved; the contrast ratio (CR) is defined as the ratio of field-on and field-off output light intensities. It should be noted that the linear light polarization at the output is conserved only for a particular orientation of the polarization vector at the input and only at a particular wavelength. For example, data shown in Figure 1 are obtained for the vector **e** at the layer input oriented at an angle of $\alpha = -60$ deg to the x-axis and field E_x. This results lead to interesting spectral features of the electrooptic effect.

Figure 2a shows the polarization states of light of different wavelength ($\lambda = 450$–650 nm with a step of 25 nm) transmitted through the liquid crystal layer at $E = 0$. One can see a strong dispersion of the polarization states; the polarization states are considerably spread along the equator. Therefore, the high contrast ratio of the electrooptic response is only observed in a very narrow spectral range, see Figure 2b. As all polarizations are almost linear (all points are close to equator), the maximum transmission may easily be obtained by rotation of the analyser as illustrated by curves 1–4 in Figure 2. However, the absolute maximum of the contrast is reached only at a particular wavelength, namely, for the point located strictly on the

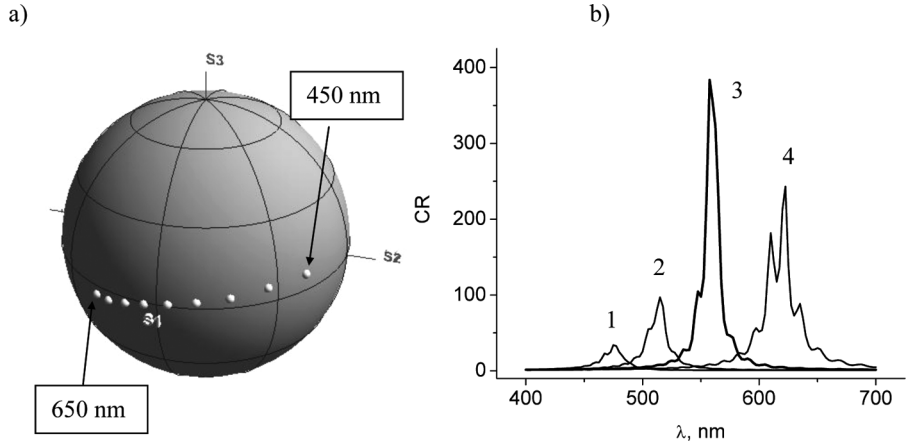

Figure 2. Calculated wavelength dependence ($\lambda = 450$–650 nm) of polarization states of the light transmitted by a chiral nematic layer for $E = 0$ (a) and spectra of the contrast ratio (b) for $E = 1\,\mathrm{V}/\mu\mathrm{m}$ and different orientation angle β for the analyser transmission axis: $\beta = 110$ deg (curve 1), $\beta = 100$ deg (2), $\beta = 0$ (3) and $\beta = 80$ deg (4). Azimuthal angle for electric vector of incident light $\alpha = -60$ deg, optical anisotropy $\Delta n = 0.2$.

equator (in our case, $\lambda = 560$ nm as seen in Fig. 2b). Further, if we change the angle α of the input polarization, the output polarization will also be changed and the maximum contrast will be observed at another wavelength.

The spectral dispersion of polarization states in the zero field can efficiently be controlled by variation of the optical anisotropy Δn. The polarization states in the range of $\lambda = 450$–650 nm are shown in Figure 3 a,b for two liquid crystals, with $\Delta n = 0.1$ and 0.05, respectively. The spread of the points along the equator becomes considerably smaller with decreasing Δn that results in broadening the spectral range of the electrooptic response illustrated by curves 1 and 2 in Figure 3c. Resuming, the spectral position of the maximum of the response is governed by variation of the axes of a polarizer and an analyser while the width of the spectral range of the light

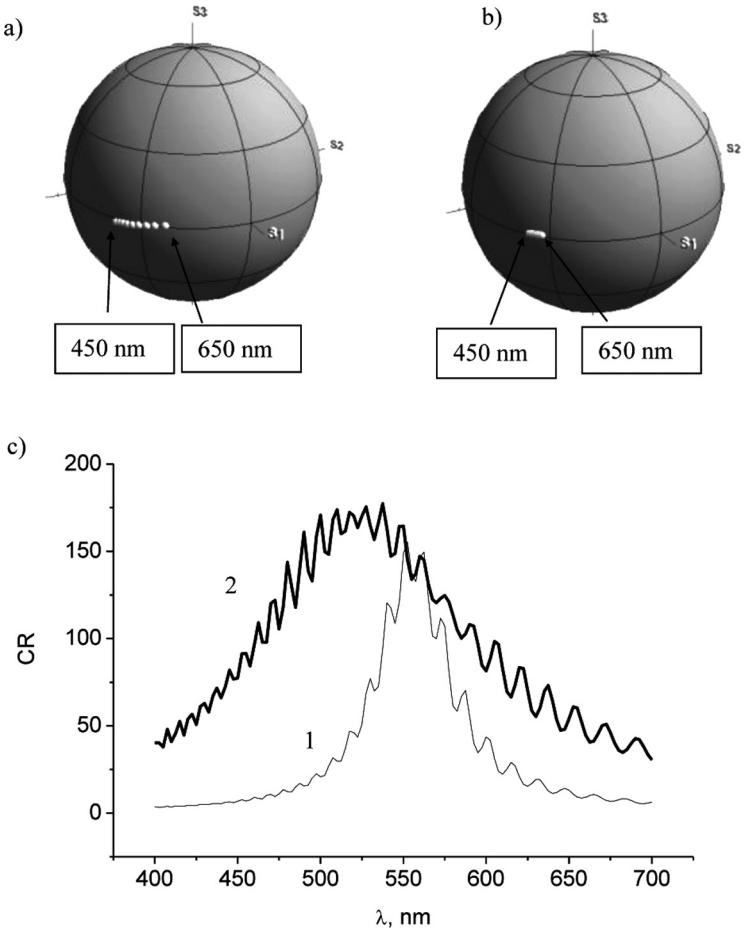

Figure 3. Calculated wavelength dependence ($\lambda = 450$–650 nm) of polarization states of the light transmitted by a chiral nematic layer at $E = 0$ for two liquid crystals with different optical anisotropy: (a) $\Delta n = 0.1$, $\alpha = -40$ deg; b) $\Delta n = 0{,}05$, $\alpha = -30$ deg. Spectra of contrast ratio for electrooptic response (c): $\Delta n = 0.1$, $\alpha = -40$ deg, $\beta = 65$ deg, $E = 1\,\mathrm{V}/\mu\mathrm{m}$ for curve 1 and $\Delta n = 0.05$, $\alpha = -30$ deg, $\beta = 64$ deg, $E = 1.5\,\mathrm{V}/\mu\mathrm{m}$ for curve 2. The oscillations are due to multiple reflections from the layer boundaries.

modulation is controlled by a change in optical anisotropy. Our modelling also shows that the spectral width increases with decreasing helical pitch. We shall come back to this point when discussing experimental data.

Another principal feature of the anharmonicity effect is short times of inducing and relaxation of high spatial harmonics in the helical structure of the director and, consequently, a fast change of the light polarization states caused by field switching. The calculated electrooptic response (a change of the transmission coefficient) of the liquid crystal cell to the rectangular waveform of the electric field is shown in Figure 4a. The field of different strength is switched on within the time interval 1–3 ms and the switched-on and -off times (τ_{on} and τ_{off}) have been found as 90% of the growth or decay duration. As seen in Figure 4b, both $\tau_{on} \cong 500\mu s$ (curve 1) and $\tau_{off} \cong 280\mu s$ (curve 2) slightly depend on the electric field strength up to $E = 1\,V/\mu m$ but, at higher fields, τ_{on} decreases and τ_{off} increases. The calculated dependence of both times on the helical pitch is close to quadratic, $\tau \sim P^2$; for example, for $P = 0.6\,\mu m$ $\tau_{on} \cong 80\mu s$.

It should be noted that relaxation times of the anharmonicity effect are, at least, one order of magnitude shorter than characteristic times of electrooptic effects in nematic liquid crystals because, in our case, the director relaxation is determined not by the thickness of the liquid crystal layer (d about few microns) but mostly by the spatial period of the induced 3rd harmonic ($m = 3$) that is three times smaller than P. Note, that the relaxation time are proportional to the period squared. As an estimate of the relaxation time for the anharmonicity effect one can use a relationship

$$\tau_{off} \cong \xi \frac{\gamma}{K_{22}(mq)^2} \equiv \xi\tau \tag{11}$$

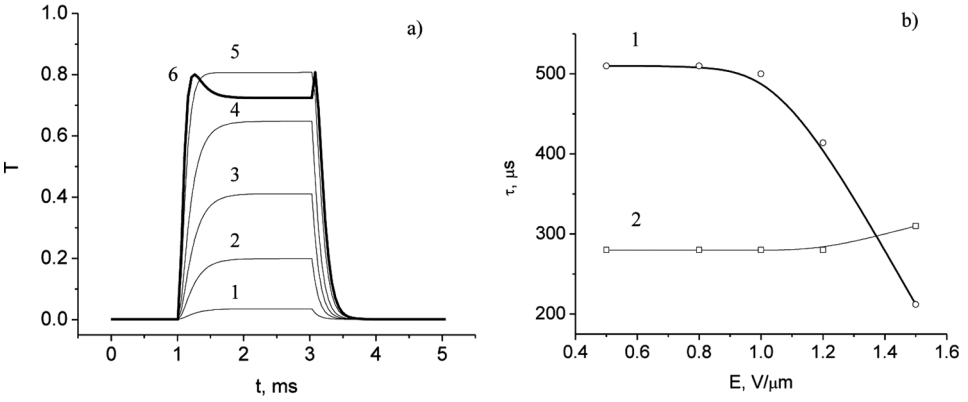

Figure 4. (a) Calculated time dependence of field-induced transmission for a model structure including a liquid crystal layer and an analyser. The data are given for a normally incident linearly polarized light ($\alpha = -60$ deg, $\lambda = 550$ nm). A rectangular field pulse applied within time interval $t = [1, 3]$ ms. The field strength in V/μm is as follows: 0.5 (curve 1), 0.8 (2), 1 (3), 1.2 (4), 1.5 (5) and 1.7 (6). (b) Dependences of switch-on (1) and –off (2) times on the pulse field strength. The liquid crystal layer parameters: $d = 8\,\mu m$; $\Delta n = 0{,}2$; $K_{22} = 5$ pN; $\gamma = 0{,}1$ Pas; $P = 1.2\,\mu m$; $\Delta\varepsilon = 15$.

where $q = 2\pi/P$, $m = 3$, K_{22} is twist elastic modulus and γ rotational viscosity. Factor $\xi \cong 3.5$ relates the technical criterion mentioned above (90% of the pulse edge duration) to time τ (exponential factor) of director elastic relaxation.

3. Experiment

3.1. *Liquid Crystal Cell*

The scheme of experimental cells is pictured in Figure 5. A liquid crystal layer is placed between two glass plates (2), one of which is supplied by a system of 20 μm wide interdigitated chromium electrodes (3) having full period of 40 μm. The total area of the patterned structure is $4 \times 4\,\text{mm}^2$. Both plates have been covered with alignment polyimide layers (4) and rubbed in the opposite directions so that a chiral liquid crystal forms a planar Grandjean texture with the helical axis along the cell normal. The rubbing direction formed the angle of 45 deg with respect to the field direction and the cell thickness $d = 17.5 \pm 0.1$ μm was fixed by insulating spacers (5) located outside of the electrode pattern. The field strength discussed throughout the paper is related to the electrode plane but, in fact, the electric field is not uniform within the bulk of the cell. This should be taken into account when the experimental data are compared with calculations assuming the uniform in-plane field everywhere. The cell is placed between two polarizers (6).

The bipolar, rectangular, voltage pulses of varied frequency, duration and duty time were synthesized using voltage generator G5-30A (Russia). The control of quality of the liquid crystal texture and electrooptic measurements were carried out using a set-up based on a polarisation microscope [7] with either a 20 W incandescent lamp or a He-Ne laser ($\lambda = 633$ nm) as light sources. When necessary, the narrow band

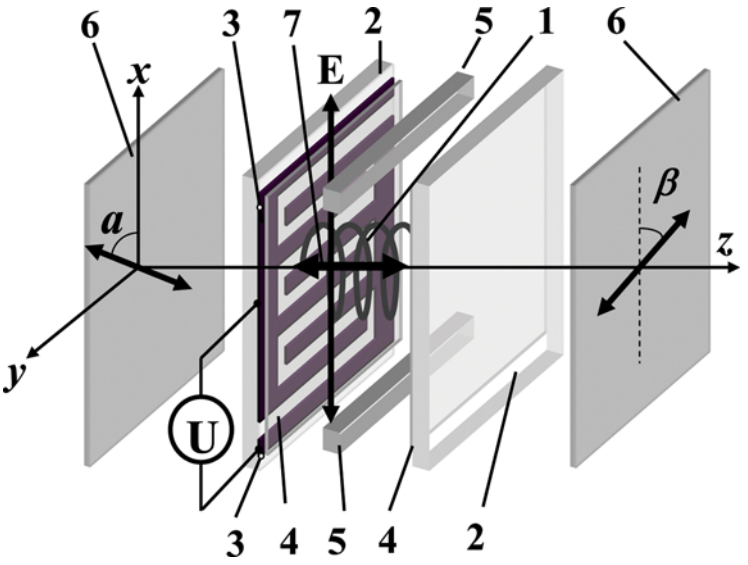

Figure 5. Scheme of an electrooptic cell placed between two polarizers: chiral nematic layer (1), glass substrates (2), interdigitated electrodes (3), polymer alignment films (4), insulating spacers (5), polarizers (6), arrow showing the orientation of the helix axis (7). U and **E** are voltage source and the electric field vector. (Figure appears in color online.)

($\Delta\lambda = 8$ nm) interference filters were used having maximum transmission at 464 and 533 nm. The light transmitted by the cell was detected by a photomultiplier and stored by an oscilloscope (Tektronix 3012). The spectral dependences of the transmission were measured by an automatic spectrometer MDR-23 (Russia) controlled by software "PhysLab" developed in the laboratory.

3.2. *Liquid Crystal Materials*

Chiral liquid crystal mixtures were prepared on the basis of commercial achiral nematic materials from Merck. Their parameters are listed in Table 1. To induce chirality and vary the pitch P, we use as a chiral dopant an optically active compound a-bis(2-chlorine-4-methylpentyl)biphenyl-4,4′-dicarboxylate in different concentrations.

Some values of optical and dielectric anisotropy of nematic liquid crystals presented in Table 1 is used also for chiral nematics because the difference between chiral and achiral counterparts may reach less than 15% at the maximum concentration of the chiral dopant (for compounds with high anisotropy Δn and $\Delta\varepsilon$ the mentioned difference is even smaller). The pitch of the helix has been measured from the Grandjean zones in wedge form cells. The accuracy was about 0.1 μm for the pitches in the vicinity of $P \approx 1$ μm. In all our experiments the selective reflection bands were in the near infrared range ($\lambda < 0.8$ μm).

4. Experimental Results and Discussion

Generally, the linearly polarized light transmitted by a chiral nematic layer become elliptically polarised. However, as shown by modelling and experiments, for particular angles of the linear polarisation of a given wavelength at the input, we can have the linear polarization at the output as well. Such polarization is blocked by a linear analyser, however, upon application of the electric field, the cell becomes transparent again. The correspondent contrast ratio (CR) characterises the quality of the device. Figure 6 demonstrates dependences of CR for three experimental cells as functions of the electric field at a fixed light wavelength $\lambda = 633$ nm. The dependences are monotonic and the maximum values of CR in all cases exceed 750. Such a high contrast allows the anharmonicity effect to be considered as a serious candidate for technical applications. Note that, in accordance with numerical modelling, the contrast ratio clearly manifests a spectral dependence. In Figure 7, such a dependence shown for sample Ch-IPS-17 from Table 1 embraces only a part (FWHM ≈ 100 nm) of the visible range. However, we may control the width of that band varying orientation of polarizers and optical anisotropy of a material. In the next figures, for clarity, we will use the values of CR for different samples normalised to the unity. In Figure 8 and 9 the normalised CR for materials Ch-IPS-16 and Ch-IPS-20 are given as functions of angle α the polarizer forms with respect to electric field E_x. The experimental procedure was as follows. The angle α was varied with steps of 5 deg and, for each step,

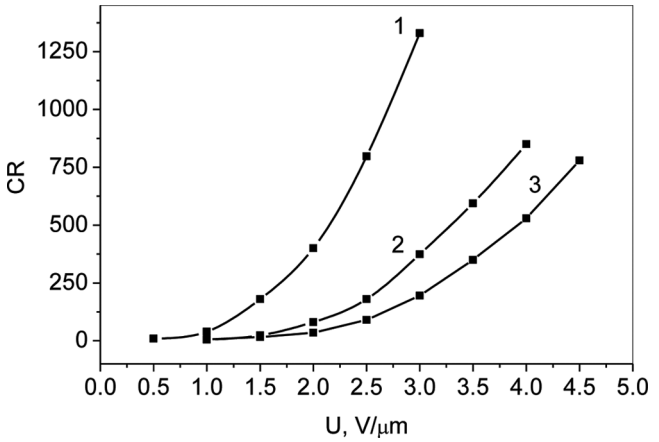

Figure 6. Field dependence of the contrast ratio for materials with different dielectric and optical anisotropy (angles α and β define orientation of transmission axes of polarizer and analyzer, respectively): Curve 1: Ch-IPS-13 ($\alpha = 10$ deg, $\beta = 0$, $\Delta n = 0.22$, $\Delta\varepsilon = 14.5$); Curve 2: Ch-IPS-20 ($\alpha = 40$ deg, $\beta = -20$ deg, $\Delta n = 0.12$, $\Delta\varepsilon = 7$); Curve 3: Ch-IPS-16 ($\alpha = 45$ deg, $\beta = -33$ deg, $\Delta n = 0{,}052$, $\Delta\varepsilon = 2.5$).

we searched that value of the angle β the analyser forms with respect to E_x, which provides minimum transmission in the zero field. The dependencies $\beta(\alpha)$ appear to be straight lines. Finally we find the maximum of CR upon applying the field.

For sample Ch-IPS-16 having small $\Delta n = 0.0517$ (Figure 8) the maximum contrast at $\lambda = 464$, 533 and 633 nm has been reached, at the angles α in the range of $40 \div 50$ deg and β at $-22 \div -33$ deg. For sample Ch-IPS-20 having $\Delta n = 0.129$ (Figure 9), at the same wavelengths, the range of the optimum angles α is essentially wider (20–40 deg) and angles β are in the range of $-5 \div -19$ deg. Thus, an increase

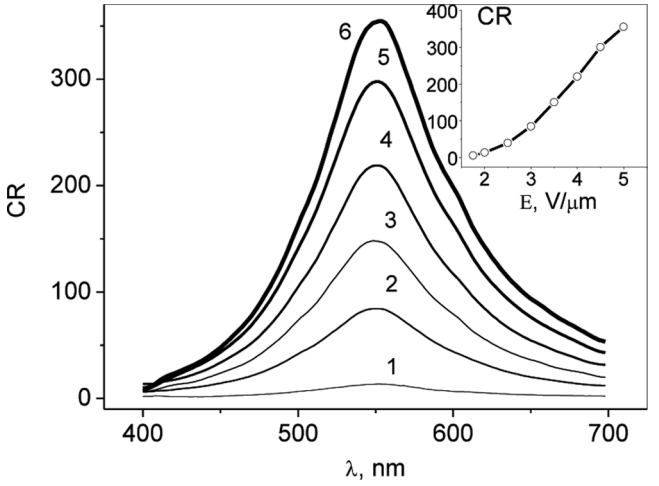

Figure 7. Spectral dependence of contrast ratio (CR) for different fields E in V/μm: 2 (curve 1), 3 (2), 3.5 (3), 4 (4), 4.5 (5), 5 (6). Inset: maximum CR at $\lambda = 553$ nm as a function of field strength. Sample Ch-IPS-17, $\alpha = 45$ deg, $\beta = -30$ deg.

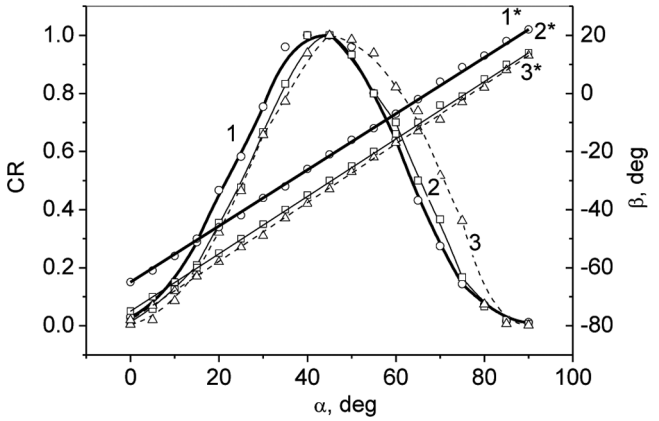

Figure 8. Normalized contrast ratio (CR, curves 1–3) as a function of angle α of the polarizer transmission axis. Straight lines 1*–3* show orientation of the analyser transmission axis β, at which the maximum CR is realized. Dependences 1 (1*), 2 (2*) and 3 (3*) are plotted for $\lambda = 464$, 553 and 633 nm, respectively. Sample Ch-IPS-16 ($\Delta n = 0.052$), temperature $T = 23°C$, field $E = 4\,V/\mu m$.

of the optical anisotropy results in a stronger dispersion of the polarization states and CR as predicted by numerical calculations, see Figures 2 and 3. The spectral shift of CR following a change of the analyzer axes β is also in agreement with modeling, as demonstrated in Figure 10 for sample Ch-IPS-16. In this case, the angle $\alpha = 45$ deg is fixed, and β is varied, but the inverse situation also results in the shift of CR spectra on the wavelength scale.

Therefore, we confirm the results of numeric calculations. Indeed, the decisive factors that influence the width of the spectral range of efficient light modulation are the optical anisotropy and the pitch of the helix. In Figure 11 the spectral dependences of normalized CR are given for the fixed pitch $P = 1\,\mu m$ and varied optical anisotropy. For large value of $\Delta n = 0.22$ (Ch-IPS-13, curve 1) the spectral range of

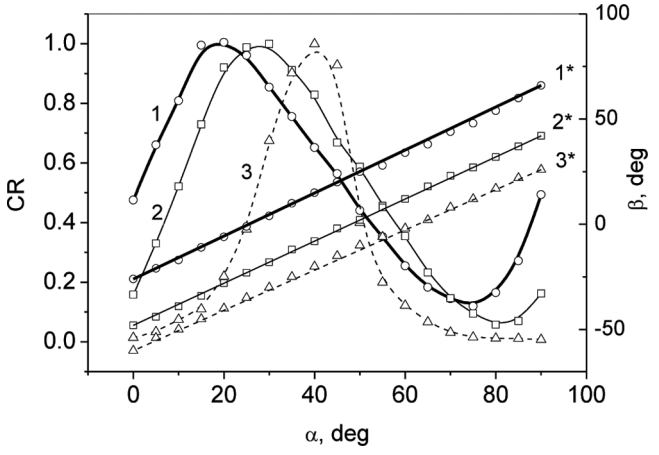

Figure 9. Same as in Figure 8 for the sample Ch-IPS-20 ($\Delta n = 0.12$), $T = 23°C$, $E = 3\,V/\mu m$.

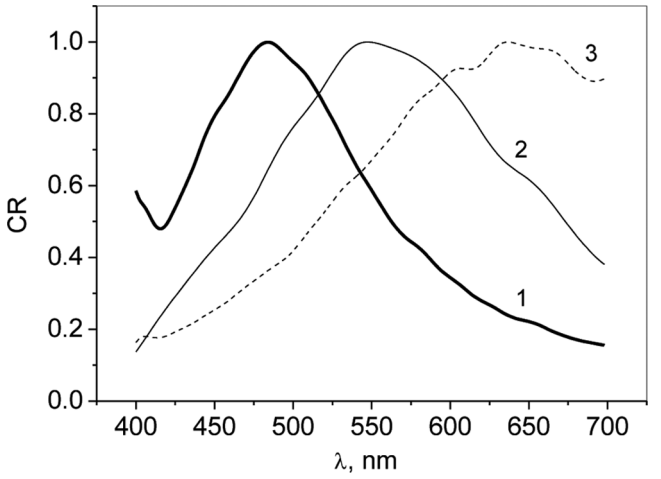

Figure 10. Normalized contrast ratio spectra (CR, curves 1–3) for different angles β of the analyser transmission axis: $\beta = 36$ deg (curve 1), $\beta = 38$ deg (curve 2) and $\beta = 40$ deg (curve 3). Sample Ch-IPS-16 ($\Delta n = 0.052$), $\alpha = 45$ deg, $T = 23°C$, $E = 5\,V/\mu m$.

high contrast becomes very narrow ($\Delta\lambda \sim 15$ nm); with decreasing Δn the range $\Delta\lambda$ dramatically increases. For $\Delta n = 0.053$ (curve 4) the effective modulation is observed over the essential part ($\sim$250 nm) of the visible range. Unfortunately, to obtain a high brightness and CR > 100 one needs a significant thickness ($d > 30\,\mu m$) of the liquid crystal layer. In reality, we should operate with thickness of 15–20 μm in order to keep homogeneity of the electric field. Then the contrast ratio can be reduced down to 30 at the edges of the range 400–700 nm with the maximum CR = 70 at $\lambda = 550$ nm, see curve 4 for sample Ch-IPS-16 in Figure 11.

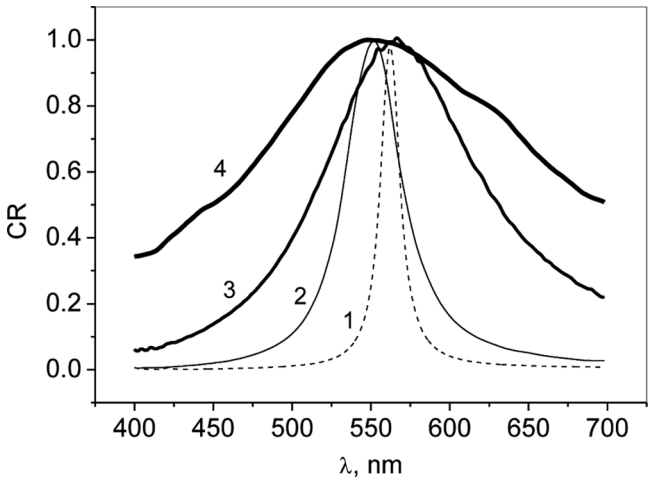

Figure 11. Normalized contrast ratio spectra for liquid crystals with different optical anisotropy. Curve 1: sample Ch-IPS-13, $\Delta n = 0.22$ ($\alpha = 0$, $\beta = -160$ deg); Curve 2: sample Ch-IPS-20, $\Delta n = 0.12$ ($\alpha = 30$ deg, $\beta = -18$ deg); Curve 3: sample Ch-IPS-2, $\Delta n = 0.075$ ($\alpha = 45$ deg, $\beta = -27$ deg); Curve 4: sample Ch-IPS-16, $\Delta n = 0.052$ ($\alpha = 45$ deg, $\beta = -30$ deg).

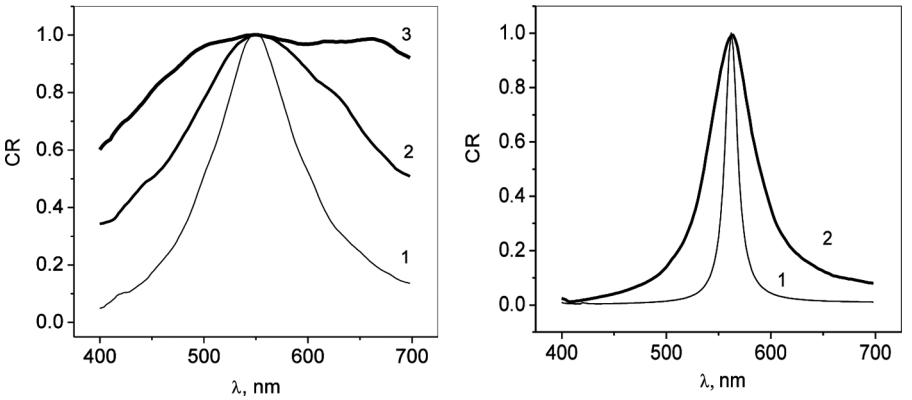

Figure 12. Normalized contrast ratio spectra for liquid crystals with different pitch of the helix. (a) Low optical anisotropy $\Delta n = 0.052$; Curve (1): $P = 2\,\mu m$ (Ch-IPS-17, $\alpha = 45$ deg, $\beta = 30$ deg); Curve (2): $P = 1\,\mu m$ (Ch-IPS-16, $\alpha = 45$ deg, $\beta = 30$ deg); Curve (3): $P = 0.6\,\mu m$ (Ch-IPS-15, $\alpha = 45$ deg, $\beta = 38$ deg). (b) High optical anisotropy $\Delta n = 0.22$; Curve (1):

As to the role of a helical pitch, it is clear from Figure 12a,b where pitch dependent contrast ratio spectra are demonstrated for two materials having different optical anisotropy ($\Delta n = 0.22$ and $\Delta n = 0.0517$). The pitch was varied within 0.6–2 μm. In both (*a*) and (*b*) cases, the spectral range of efficient modulation is expanded essentially with decreasing pitch. For small pitch and small optical anisotropy, the CR is almost wavelength independent within 500–700 nm.

The oscillograms of the electrooptic response to the rectangular voltage pulses of 2.5ms duration are shown in Figure 13 for two chiral nematics (Ch-IPS-13 and Ch-IPS-16) having different Δn. As predicted above, the response is very fast as compared to conventional effects on nematic liquid crystals. The switch-on and -off

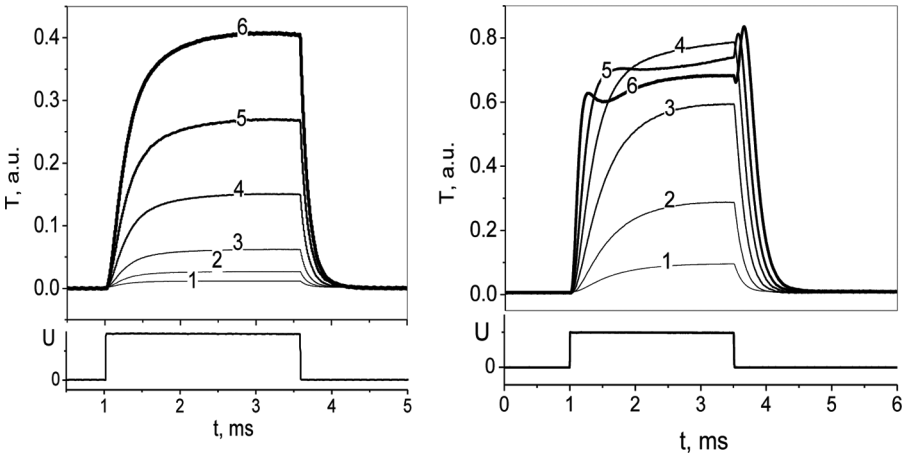

Figure 13. Time dependence of electrooptic response of samples Ch-IPS-16 (a) and Ch-IPS-13 (b) to rectangular pulse of different field strength *E*. Curves 1–6 corresponds to the range of *E* from 1.5 to 4 V/μm with a step of 0.5 V/μm.

Table 2. Switching times at voltage $U = 50$ V for different samples

Sample	Switch-on time (τ_{ON},μs)	Switch-off time (τ_{OFF},μs)
Ch-IPS-13	990 (400 μs for $U = 70$ V)	400
Ch-IPS-16	620	250
Ch-IPS-15	200	120

times are in the sub-millisecond range, see Table 2. For Ch-IPS-13 $\tau_{on} = 990$ μs for pulse amplitudes U = 50 V and reduces more than two times (down to 400 μs) at a voltage of 70 V. These data agree very well with the numerical results obtained for a liquid crystal with $\Delta\varepsilon = 15$ and $P = 1.2$ μm, the values close to the experimental ones, $\Delta\varepsilon = 14.5$ and $P = 1$ μm (Ch-IPS-13). The switch-off time ($\tau_{off} = 400$μs) are also close to results of modelling (280 μs); some discrepancy is expected because such parameters as elastic moduli and viscosity of our mixtures are known only approximately. With decreasing helical pitch down to 0.6 μm we obtain $\tau_{off} \approx 100$μs (sample Ch-IPS-15 in Table 2). This value is one order of magnitude better than the switching times achieved today on nematic liquid crystals that opens up prospects for applications of the anharmonicity effect in displays and other electrooptic devices.

5. Conclusion

A new electrooptic effect based on the distortion of the helical structure in chiral nematic layers has been studied in detail. It is shown that the electric field induced spatial harmonics in the initially sine-form distribution of the director result in essential change of the polarization state of light transmitted through a thin liquid crystal layer. The general spectral features of the effect have been studied both experimentally and using numerical simulations. A decrease of both the optical anisotropy and the helical pitch of a liquid crystal was shown to reduce the spectral dispersion of transmitted light polarization states and, as a result, to broaden the spectral range of efficient light modulation. The effect studied is very fast because its relaxation time is determined not by the layer thickness but by essentially smaller parameter, namely, the spatial period of the third harmonic induced in the helical structure of the director. The latter allowed us to realize fast switching of the corresponding electrooptic devices with characteristic times one order of magnitude lower as compared to known electrooptic effects based on nematic liquid crystals.

Acknowledgment

The work is supported by Russian Academy of Sciences (Phys. Dept.) in framework of the program "Physics of new materials and structures".

References

[1] Kats, E. I. (1970). *Zh. Eksp. Teor. Fiz.*, *59*, 1854.
[2] Kopp, V. I., Zhang, Z.-Q., & Genack, A. Z. (2003). *Progr. Quant. Electron.*, *27*, 369.
[3] Yeh, P., & Gu, C. (1999). *Optics of Liquid Crystal Displays*, J. Wiley & Sons. Inc.: New York.

[4] Kobayashi, S., Shimojo, T., Kasano, K., & Tsunda, I. (1972). *SID Symp. Digest of Technical Papers*, 68.
[5] Soref, R. A. (1974). *J. App. Phys.*, *45*, 5466.
[6] Ozaki, M., Tagawa, A., Sadohara, Y., Oda, S., & Yoshino, K. (1991). *Jpn. J. Appl. Phys.*, *30*, 2366.
[7] Barnik, M. I., & Palto, S. P. (2004). *Ferroelectric*, *310*, 155.
[8] Kiefer, R., Weber, B., Windscheid, F., & Baur, G. (1992). *Intern. Conf. Japan Display,' 92*, Proceedings, 547.
[9] Baur, G. (1993). *22 Freiburher Arbeitstagung Flussigkristalle*, Abstracts, O1, Freiburg, April.
[10] Broughton, B. J., Clarke, M. J., Blatch, A. E., & Coles, H. J. (2005). *J. Appl. Phys.*, *98*, 034109.
[11] Palto, S. P. (2001). *JETP*, *92*, 552.
[12] Palto, S. P. (2003). *Crystallography Reports*, *48*, 124.
[13] Berreman, D. W. (2007). *J. Opt. Soc. Am.*, *62*, 502.
[14] Palto, S. P. (2002). *JETP*, *94*, 260.
[15] Belyakov, V. A., & Kats, E. I. (2000). *JETP*, *91*, 488.